GT2020-16091

EFFECT OF AN AZIMUTHAL MEAN FLOW ON THE STRUCTURE AND STABILITY OF THERMOACOUSTIC MODES IN AN ANNULAR COMBUSTOR MODEL WITH ELECTROACOUSTIC FEEDBACK

Sylvain C. Humbert[1][*]**, Jonas P. Moeck**[2]**, Alessandro Orchini**[1]**, Christian Oliver Paschereit**[1]

[1]Chair of Fluid Dynamics, Technische Universität Berlin, Berlin, Germany
[2]Department of Energy and Process Engineering, Norwegian University of Science and Technology, Trondheim, Norway

ABSTRACT

Thermoacoustic oscillations in axisymmetric annular combustors are generally coupled by degenerate azimuthal modes, which can be of standing or spinning nature. Symmetry breaking due to the presence of a mean azimuthal flow splits the degenerate thermoacoustic eigenvalues, resulting in pairs of counter-spinning modes with close but distinct frequencies and growth rates. In the present study, experiments have been performed using an annular system where the thermoacoustic feedback due to the flames is mimicked by twelve identical electroacoustic feedback loops. The mean azimuthal flow is generated by fans. We investigate the standing/spinning nature of the oscillations as a function of the azimuthal Mach number for two types of initial states, and how the stability of the system is affected by the mean azimuthal flow. It is found that spinning, standing or mixed modes can be encountered at very low Mach number, but increasing the mean velocity promotes one spinning direction. At sufficiently high Mach number, only spinning modes are observed in the limit cycle oscillations. In some cases, the initial conditions have a significant impact on the final state of the system. It is found that the presence of a mean azimuthal flow increases the acoustic damping. This has a beneficial effect on stability: it often reduces the amplitude of the self-sustained oscillations, and can even suppress them in some cases. However, we observe that the suppression of a mode due to the mean flow may destabilize another one. We discuss our findings in relation with an existing low-order model.

NOMENCLATURE

Roman

$\boldsymbol{A}$, $a_{j,k}$	Acoustic frequency response matrix and its component
$\boldsymbol{B}$, $b_{j,m}$	Modal basis matrix and its component
c	Speed of sound
$\boldsymbol{C}$, $c_{m,j}$	Modal response matrix and its component
$\boldsymbol{D}$, $\boldsymbol{E}$, $\boldsymbol{F}$	State-space model matrices
f	Frequency
h	Coefficient of the power-law velocity profile
$\boldsymbol{I}$	Identity matrix
i	Imaginary unit $\sqrt{-1}$
j	Tube index
M	Mach number
m	Azimuthal mode number
N	Number of tubes
n	Flame model gain
$\boldsymbol{p}$	Pressure vector
$\boldsymbol{q}$	Flame model output vector
r	Radial coordinate
R	Mean radius of the annular cavity
R_{in}	Radius of the inner annulus
R_{out}	Radius of the outer annulus
Re	Reynolds number

---

[*]corresponding author: sylvain.humbert@tu-berlin.de

s	Laplace variable
$\bar{u}_\theta$	Mean azimuthal velocity
$\boldsymbol{u}$	RTC output/loudspeakers input vector
t	Time
x	Damped harmonic oscillator variable
$\boldsymbol{y}$	Microphone output voltage vector
z	Axial coordinate

Greek

α	Damping coefficient
δ	Saturation limit
ζ	Linear damping factor
θ	Angular coordinate
σ	Growth rate
τ	Flame model time delay
ω	Angular frequency
$\Delta\omega$	Width of the resonant peak

Superscripts

$\hat{(\cdot)}$	Fourier transform
$\dot{(\cdot)}$	First time derivative
$\ddot{(\cdot)}$	Second time derivative
$(\cdot)^{\pm}$	Co- and counter-swirl component

Abbreviations

EAF	Electroacoustic feedback
FTF	Flame transfer function
IC	Initial condition
LES	Large eddy simulations
RTC	Real-time controller

INTRODUCTION

The use of lean-premixed combustion technology in gas turbine combustors, aimed at reducing the NOx emissions, often leads to thermoacoustic instabilities that arise from the constructive interaction between the acoustics of the combustor and the fluctuating heat release rate from the flame. The resulting self-sustained oscillations can lead to unwanted phenomena, such as structural damage and flame flashback or blow-off. Therefore, their avoidance should be a priority from the design stage. To this end, thermoacoustic phenomena have been studied intensely in the context of gas turbine combustion [1, 2]. In axisymmetric annular combustors, where multiple burners are connected to a single ring-shaped cavity, thermoacoustic instabilities are generally associated with degenerate azimuthal modes. They can be described in the linear regime by pairs of standing or counter-spinning modes that share the same frequency and that grow exponentially at the same rate. When the oscillations reach a finite amplitude level, they start to be affected by the nonlinear flame response, which makes both modes interact and compete. When a degenerate pair of modes is linearly unstable, the ratio of their respective amplitudes is conserved during the whole linear regime. Therefore the ratio of the amplitudes of both components is equal to the initial amplitude ratio when nonlinear effects appear. This is generally close to unity if the initial state contains only broadband noise. It is then the nonlinear flame response that determines whether the modal competition scenario leads to periodic oscillations of standing, spinning or mixed nature.

However, the symmetry can be broken for various reasons. For example, it has been shown numerically [3, 4] and experimentally [5–7] that an axisymmetric arrangement of multiple co-swirling injectors produces a non-zero azimuthal bulk flow in the annular cavity. This breaks the reflection symmetry between the co-swirl spinning mode and the counter-swirl spinning mode, i.e. the spinning modes that propagate with and against the flow, respectively. Theoretical studies demonstrate that this splits the degenerate thermoacoustic eigenvalues, resulting in pairs of counter-rotating modes with close but distinct frequencies and growth rates [8–10]. Experimental evidence of acoustic eigenvalue splitting due to an azimuthal flow is provided in [11] for a ring cavity, while in the field of thermoacoustics, eigenvalue splitting of the first transverse acoustic mode due to the presence of swirl has been observed in a cylindrical flame tube in a cold experiment [12].

Eigenvalue splitting is a linear mechanism that has consequences on the final state of thermoacoustic oscillations. In particular, the standing/spinning nature of the modes in a system with azimuthal mean flow is generally different from the zero-Mach-number configuration. For example, it is observed in the large eddy simulations (LES) of [3] that the two counter-spinning modes coexist, but the mode which spins in the direction of the bulk flow dominates. On the other hand, in the study of [4], the dominant mode is a standing mode that slowly rotates at the mean flow speed, but occasional switching to spinning modes appears. Nevertheless, a general challenge associated with the short physical simulation times in LES is that it does not provide any general conclusion about the mode nature that predominates out of these operating conditions. From the experimental side, a closer look at the mean velocity profile generated by multiple swirlers in [6] indicates that the mean azimuthal flow direction depends on the radial coordinate. It is found that it is the mean flow direction at the location of the heat release peak that drives the mode nature: if the peak of heat release is encountered in the central region, where the mean flow approaches zero, a standing mode is observed; on the contrary, if the peak is encountered in a region close to the inner or outer wall, where the mean azimuthal flow is not negligible, a spinning mode is encountered. Its propagation direction follows the mean flow direction in that region [6]. One can then expect that in the presence of a unidirectional mean azimuthal flow, the dominant mode should be spinning in the mean flow direction. In contrast to these observations, it has recently been shown analytically, under simplifying assumptions and considering a cubic saturation model, that a uniform mean flow should promote the counter-swirl spinning

mode [10], even though both counter-spinning modes are found to be stable solutions below a critical Mach number value.

In the present experimental study, we investigate the effect of a mean azimuthal flow on self-sustained oscillations in an annular system with electroacoustic feedback (EAF), presented in [13]. The setup incorporates the EAF concept, first introduced for a single cavity in [14,15], into the annular rig of [16–18]. In each tube, the thermoacoustic feedback of a flame is mimicked by delaying and filtering the fluctuating pressure signal and sending the resulting signal to a loudspeaker that acts as an acoustic source. This allows us to study self-excited oscillations in a well-defined, low-noise environment, comparable to systems with combustion. Furthermore, the flame model parameters and the mean flow velocity can be varied in a precise and flexible manner. The absence of heat sources allows us to close the outlet of the annular cavity with a hard wall, thus producing a realistic downstream acoustic boundary condition, similar to that of a choked outlet. The azimuthal mean flow is generated by computer fans, similarly to [11].

In this study, we first present the effect of an azimuthal mean flow on the acoustics and on the stability of the self-sustained oscillations. Then, we address the standing/spinning mode nature that is promoted by an azimuthal flow. We compare our experimental results with theoretical predictions from [10].

1 EXPERIMENTAL SETUP AND MODELING

The experimental setup is presented in Fig. 1. It consists of an annular cavity, closed at the top, connected to $N = 12$ tubes mimicking the burners, open at the bottom. A microphone (GRAS 40BP), which measures the pressure fluctuations, and a loudspeaker (Monacor KU516, 160-6500Hz) are attached to each tube. The EAF is produced in each tube via a real-time controller (RTC: dSPACE1103) by passing the pressure signal to a transfer function and saturating its output. The RTC output signal is amplified (t-Amp E4-130) and sent to a loudspeaker that generates acoustic waves. A sampling frequency of 10 kHz is used for the recording of the microphone signals and for the EAF. The microphones and the loudspeakers have been calibrated relative to each other to achieve 12 nominally identical EAF loops.

To introduce symmetry breaking due to azimuthal mean flow effects, we use twelve fans (San Ace 60) located in the annular chamber between each pair of annulus–duct connections, thus preserving the discrete rotational symmetry of the system. The reflection symmetry is also preserved when the fans are off. A calibration linking the bulk Mach number to the total power sent to the fans has been performed using a Pitot tube at 6 axial locations, placed at the middle between the inner and the outer annulus ($r = R = (R_{in} + R_{out})/2$). The radial profile of the mean azimuthal velocity is assumed to follow a $1/h$ power law [19]. An integration over the radial coordinate at a given axial location
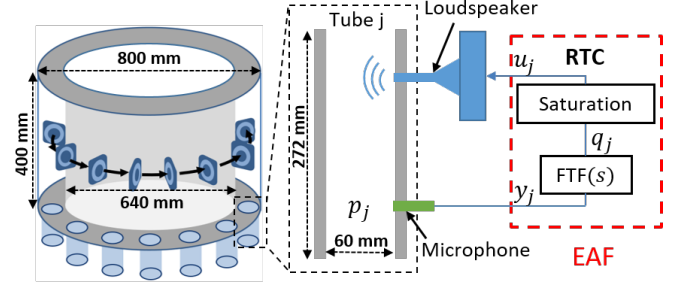

FIGURE 1: Experimental setup. Left: the annular setup with fans. Right: details on the EAF loop. An identical feedback loop is present in each tube.

z leads to

$$\frac{1}{R_{out} - R_{in}} \int_{R_{in}}^{R_{out}} \overline{u}_\theta(z,r)dr = \frac{h}{h+1}\overline{u}_\theta(z,R) \qquad (1)$$

and h is estimated by $h \approx 1.5\log_{10}(\text{Re}) - 1.5$, where Re is the Reynolds number. Knowing the mean flow velocity at 6 axial locations allows us to estimate the bulk flow velocity over a whole cross section. The bulk flow velocity obtained at the maximum fan power is about 9 m/s. The mean azimuthal velocity profile is not uniform in the axial direction. $\overline{u}_\theta(x)$ is within an interval of ±21% around the bulk flow velocity.

The system can be thought of as composed of two components: one is the acoustics of our setup, in which we also include the response of the microphones, the loudspeakers and their respective amplifiers; the other is the flame model that is imposed by the RTC. The microphone amplifier includes a second order low-pass filter with a cut-off frequency of 2 kHz, allowing to select the range of frequencies of interest for the study of azimuthal modes.

1.1 Acoustic modal frequency response

In order to assess the effects of an azimuthal mean flow on the acoustic modes, we propose to characterize experimentally the acoustics of our setup at various Mach number values. We first need to build the $N \times N$ acoustic response matrix that links the output vector $\mathbf{y}$, collecting the voltage signals y_j ($j = 1 \ldots N$) from the microphones, to the input vector $\boldsymbol{u}$ comprised of the voltage signals u_j sent by the RTC output channels to the loudspeakers. We start by determining the acoustic frequency response vector $\boldsymbol{A}_1(i\omega)$, with components $a_{j,1}$, which links in the frequency domain the output $\hat{y}_j$ to the signal sent to the loudspeaker of tube 1, $\hat{u}_1$, via

$$a_{j,1}(i\omega) \equiv \frac{\hat{y}_j(i\omega)}{\hat{u}_1(i\omega)} = \frac{\hat{S}_{y_j u_1}}{\hat{S}_{u_1 u_1}} \qquad (2)$$

where $\hat{S}_{v_1 v_2}$ is the cross power spectral density between the scalar variables v_1 and v_2. This is obtained experimentally by sending a chirp signal with a linearly increasing frequency from 160 to 700 Hz. Given the rotational symmetry of the system, we assume that an excitation signal in the tube j leads to a response in the tube $j+k$ that is identical to the response in the tube $k+1$ to an excitation in the tube 1. In other words, the response matrix $\boldsymbol{A}$ is assumed to be circulant [17,18]. Therefore, the knowledge of $\boldsymbol{A}_1$, which constitutes the first column of $\boldsymbol{A}$, is sufficient to construct the entire acoustic response matrix. The column j is obtained by shifting the components of $\boldsymbol{A}_1$ by $j-1$ rows, as follows:

$$\boldsymbol{A} = \begin{pmatrix} a_{1,1} & a_{1,2} & \cdots & a_{1,N} \\ a_{2,1} & a_{2,2} & \cdots & a_{2,N} \\ \vdots & \vdots & \ddots & \vdots \\ a_{N,1} & a_{N,2} & \cdots & a_{N,N} \end{pmatrix} = \begin{pmatrix} a_{1,1} & a_{N,1} & \cdots & a_{2,1} \\ a_{2,1} & a_{1,1} & \cdots & a_{3,1} \\ \vdots & \vdots & \ddots & \vdots \\ a_{N,1} & a_{N-1,1} & \cdots & a_{1,1} \end{pmatrix} \quad (3)$$

In order to identify the effect of the flow on each mode, it is appropriate to isolate each modal response from the other ones. To this end, the modal response matrix $\boldsymbol{C}$ is obtained by projecting $\boldsymbol{A}$ on the spinning modal basis [16] by means of the operation

$$\boldsymbol{C} = \boldsymbol{B}^{-1}\boldsymbol{A}, \quad (4)$$

where the components $b_{j,m}$ of $\boldsymbol{B}$ take the form [16]:

$$b_{j,m} = e^{-im\theta_j}, \quad (5)$$

where m is the azimuthal mode number ($m = -5 \dots 6$ in our case) and $\theta_j \equiv 2(j-1)\frac{\pi}{N}$, where j is the index associated to the considered tube. With these definitions, the components $c_{m,j}$ of $\boldsymbol{C}$ correspond to the response in the tube j to an excitation pattern of the form $e^{-im\theta}$. Notice that the knowledge of one column of $\boldsymbol{C}$ is sufficient to characterize the system since the components of the column j can be expressed as a function of the component of the first column as $c_{m,j} = c_{m,1}e^{-im\theta_j}$. From now on, each component $c_{m,1}$ is denoted by c_m for simplicity and is referred to as the modal frequency response of the mode m.

1.2 Acoustic eigenvalue identification

The knowledge of the modal frequency responses at various Mach number values is sufficient for a qualitative assessment of the effects of an azimuthal flow on the acoustic modes. Now we propose to quantify these effects, by determining how much the acoustic eigenvalues are affected as a function of the Mach number. Therefore, in this paragraph we present two methods that allow to extract the eigenvalues from the modal frequency responses.

Method 1: Analysis of the resonant peaks. The eigenfrequencies can be identified as the frequency of the resonant peaks of the modal frequency responses. For the identification of the acoustic growth rate, we associate to each peak of the modal frequency responses a linear, second order damped oscillator of the form:

$$\ddot{x} + 2\zeta\omega_0\dot{x} + \omega_0^2 x = 0 \quad (6)$$

where ω_0 is the eigenfrequency of the undamped system and ζ is the linear damping factor. For such a system, ζ can be estimated by the formula $\zeta = \frac{\Delta\omega}{2\omega_0}$ [20], where $\Delta\omega$ is the width of the resonant peak of $|\hat{x}(i\omega)|$ at half-height of the peak. Since the growth rate is $\sigma = -\zeta\omega_0$, it can be estimated as

$$\sigma = -\frac{\Delta\omega}{2} \quad (7)$$

where $\Delta\omega$ is determined from experimental data.

Method 2: Pole relocation technique. Another way of determining the eigenvalues of $c_m(i\omega)$ is to fit a scalar state space model of the form $\boldsymbol{D}(s\boldsymbol{I} - \boldsymbol{E})^{-1}\boldsymbol{F}$ onto each c_m, using a pole relocation technique [21]. Here, s is the Laplace variable where $\sigma \equiv \Re(s)$ and $\omega \equiv \Im(s)$. The determination of the poles allows to find the acoustic eigenvalues associated with each azimuthal order m. Note that various eigenvalues associated with the same azimuthal mode order can be found. They correspond to distinct longitudinal mode orders. For each azimuthal mode number, we choose a number of poles which is twice the number of resonant peaks of the modal response.

1.3 Flame model for the electroacoustic feedback

At low-amplitude excitation levels, flames respond linearly to upstream acoustic perturbations. The n–τ model [22] typically reproduces the delayed nature of the linear flame response. Therefore we adopt this model by delaying each input y_i of the RTC by a characteristic time τ and amplifying it by a factor n. The effect of an azimuthal mean flow on the flame response is neglected. Therefore, the chosen flame model is independent of the Mach number.

At finite amplitude levels, nonlinear effects make the oscillations saturate and the flame response becomes amplitude dependent. A saturation limit of the form [23]:

$$u_j(q_j(t)) = \begin{cases} q_j & \text{if } |q_j| < \delta \\ \delta\,\text{sgn}(q_j) & \text{otherwise} \end{cases} \quad (8)$$

is used in order to model the nonlinear flame response and, from a practical point of view, to prevent the pressure oscillation am-

plitude to reach a damaging level. All the EAF experiments presented in §3.2 and §3.3 are performed with the same value of saturation limit ($\delta = 0.2$ V).

2 ACOUSTIC WAVE PROPAGATION IN A 1D RING

Before investigating experimentally the effect of an azimuthal mean flow on the acoustic modes of our setup, we shall introduce the convective effect of an incompressible azimuthal mean flow on the acoustic eigenvalues by considering the planar acoustic wave propagation in the simplified case of a 1D ring of radius R (assuming that the radial and axial lengths are small with respect to the perimeter) with a uniform and constant azimuthal mean flow velocity $\bar{u}_\theta$. This will aid us in interpreting the experimental observations. The acoustic fluctuations are assumed to be small. Assuming a damping term of the form $\alpha \frac{\partial p}{\partial t}$ (where α is constant), the wave equation in a 1D ring in cylindrical coordinates, in the presence of a low Mach number ($M \ll 1$), uniform, azimuthal mean flow is

$$\frac{\partial^2 p}{\partial t^2} + 2\frac{\bar{u}_\theta}{R}\frac{\partial^2 p}{\partial t \partial \theta} + \alpha \frac{\partial p}{\partial t} - \frac{c^2}{R^2}\frac{\partial^2 p}{\partial \theta^2} = 0. \qquad (9)$$

For the derivation of this equation we refer to [10]. This simple 1D model contains several approximations, discussed later, but is nonetheless useful in understanding the effect of the mean flow on the eigenvalues.

Let the spatial and temporal dependence of the pressure fluctuation be represented by $p(\theta,t) = \sum \hat{p} e^{-im\theta + st}$, where $m > 0$ (m^+) and $m < 0$ (m^-) refer to spinning waves traveling in the mean flow direction and against it, respectively. Substituting this expression in Eq. 9 yields an eigenvalue problem in $s \equiv \sigma + i\omega$ for each m. Solving for s and recalling that $M \ll 1$, we found that the angular frequency and the acoustic growth rate of the spinning mode that propagates with and against the mean flow direction are respectively

$$\omega^\pm \approx \omega_{0_d}(1 \pm M) \qquad (10)$$

where $\omega_{0_d} = \omega_0\sqrt{1 - \frac{\alpha^2}{4\omega_0^2}} \approx \omega_0$ is the frequency of the damped system without mean flow, $\omega_0 \equiv |m^\pm|c/R$ is the angular frequency of the undamped system at vanishing Mach number, and

$$\sigma^\pm \approx -\frac{\alpha}{2}(1 \pm M). \qquad (11)$$

These solutions show the typical splitting of the eigenfrequencies [8–10], and predict that the co-swirl mode should be more damped than the counter-swirl mode when the mean flow effect

is only convective. The forms taken by the solutions indicate that both counter-spinning modes decay by the same amount in one oscillation period, $\frac{\sigma^\pm 2\pi}{\omega^\pm} = -\frac{\alpha\pi}{\omega_{0_d}}$. However, since they have distinct periods at non-zero Mach number, $\frac{2\pi}{\omega_{0_d}(1 \pm M)}$, the mode with the shortest oscillation period, i.e. co-swirl, decays faster.

3 RESULTS

In this section we present our experimental results. First, we use acoustic forcing to assess the effects of an azimuthal mean flow on the acoustic modes (§3.1). Then, we address its impact on the self-sustained oscillations, by performing EAF experiments: the damping effect is discussed in §3.2 and the effect on the standing/spinning mode nature is presented in §3.3.

3.1 Effect of an azimuthal flow on the acoustics

The method from §1.1 is applied in order to characterize the acoustic response of our setup at various values of the Mach number and, thus, to investigate the effects of an azimuthal mean flow on the acoustics. The forcing is applied in open loop. The acoustic modes that we study are described throughout this manuscript by their azimuthal mode order m. $m = 0$ corresponds to a longitudinal mode. The eigenfrequencies of the acoustic modes $m = [0,2,3,4,5,6]$ for $M = 0$ are $f_0 = [402,316,440,514,531,536]$ Hz. The $m = 1$ mode is not presented because its eigenfrequency (160 Hz) is too close to the lowest limit of the loudspeaker operating range. At this frequency, the loudspeaker response has a low amplitude and is affected by internal nonlinear effects (which are absent from the other modal responses). The axial pressure distribution of all the modes is a priori unknown since all 12 microphones are at the same axial location. Due to presence of the tubes, one should not necessarily think that the modes of order $m \neq 0$ are the "pure" azimuthal mode of the annular duct. A discussion about the mode structures is provided later in this section. Figure 2 shows the gain of the modal acoustic responses associated with the azimuthal mode numbers $m = 3$ and $m = 4$, at various values of the Mach number. The splitting of the eigenvalues can be observed by comparing the response of the co-swirl spinning mode (m^+) with that of the counter-swirl spinning mode (m^-).

Notice that at zero Mach number one would expect both counter spinning modes to have the same acoustic response due to the presumed degenerate nature of the eigenvalues. However, a mismatch can be observed between the black solid and dashed lines, suggesting that the zero-Mach number configuration is not perfectly symmetric. This can be attributed to an imperfect positioning of the fans, to the nominal asymmetry of the fan blades, and to imperfections of the annulus and tubes. Nevertheless, the small difference between the frequencies of the counter-spinning modes indicates that the degree of asymmetry remains small.
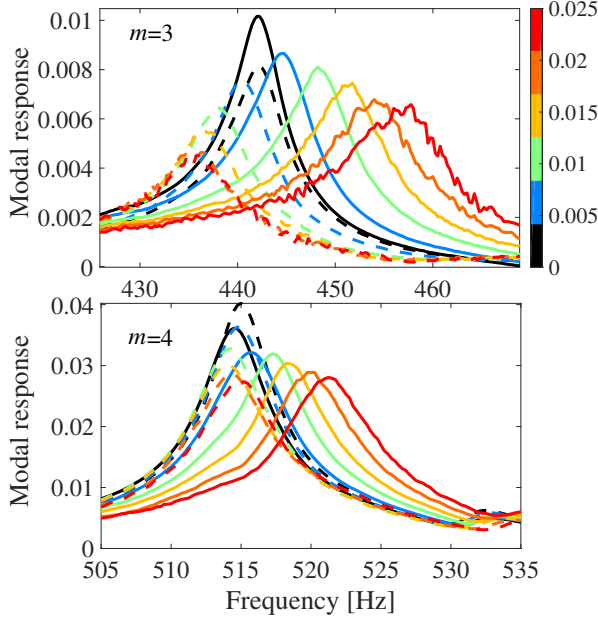
FIGURE 2: Modal acoustic responses. The colors represent different values of the Mach number. The solid and dashed lines represent the co-swirl and counter-swirl spinning components, respectively.

At non-zero mean flow velocity, the frequency gap increases with the Mach number. For both azimuthal mode numbers the frequency of the co-swirl spinning mode increases, as predicted by Eq. 10. A difference between the $m = 3$ and $m = 4$ modes can be noticed regarding the behavior of the frequency of the counter-swirl spinning mode: for $m = 3$ it decreases, as expected from Eq. 10, while for $m = 4$ it remains almost constant. One can notice that, for $m = 3$, the frequency at $M = 0$ is close to the theoretical value of the 3rd pure azimuthal mode of the chamber ($\frac{3c}{R} \approx 458$ Hz), and that the frequency splitting follows $\frac{\omega^+ - \omega^-}{\omega_{0_d}} \approx 2M$ which is in agreement with eq. 10. On the contrary, the frequency of the mode $m = 4$ is not close to the theoretical value of the pure azimuthal eigenfrequency $\frac{4c}{R}$, and the splitting $\frac{\omega^+ - \omega^-}{\omega_{0_d}}$ is much smaller than the theory. These two different behaviors suggest that the mode $m = 3$ can be thought of as the 3rd azimuthal mode of the chamber, weakly coupled with the tubes, while $m = 4$ should be, on the contrary, thought of as a fully coupled mode of the entire geometry. The frequency splitting behavior of the modes that are not shown in fig. 2 is the following. The mode $m = 2$, whose eigenfrequency is close to the theoretical value of 305 Hz has a behavior close to that of $m = 3$. Therefore it can be thought of as the 2nd azimuthal mode of the chamber weakly coupled with the tubes. The mode $m = 5$ has a behavior which is qualitatively similar to that of mode $m = 4$, with an

even smaller splitting (the splitting at $M = 0.025$ is only 2 Hz), suggesting that it is also a fully coupled mode of the entire geometry. The modes $m = 0$ and $m = 6$, which are not degenerate, have eigenfrequencies which are respectively close and not close to the theoretical values of the pure chamber modes. It suggests that $m = 0$ is the half-wave mode of the chamber weakly coupled with the tubes and that the mode $m = 6$ is a fully coupled mode. Considering the fully coupled modes of the entire geometry, one may attempt to associate the degree of coupling to the deviation of the actual frequency of the mode m with respect to the theoretical eigenfrequency of the pure m^{th} azimuthal mode of the chamber. In this respect, one may identify $m = 6$ as the mode with the highest degree of coupling.

For the study of thermoacoustic instabilities, we are interested in knowing the acoustic growth rate, which can be estimated using both methods described in §1.2. We normalize the acoustic growth rate σ of the considered mode by the mean value at zero Mach number $\sigma_{M=0} = (\sigma^+_{M=0} + \sigma^-_{M=0})/2$. Given this normalization, an increase of $\sigma/\sigma_{M=0}$, which is always positive, indicates a decrease of σ, which is always negative, reflecting an increase of the damping. The results are presented in Fig. 3 for 6 of the 7 azimuthal mode numbers detectable in our annular setup. Note also that Method 1 is not used for the co-swirl spinning mode of $m = 5$ because of the presence of a second peak close to the resonant peak considered.

The results obtained with both methods show that from $m = 0$ to $m = 5$ an increase of the Mach number tends to decrease the acoustic growth rate (increase the acoustic damping), while for $m = 6$ it remains almost constant. Moreover, we observe that the modes that should be degenerate in the vanishing Mach number limit ($m = 2..5$) have, in practice, distinct acoustic growth rates at $M = 0$. The growth rate trends of these modes show that the Mach number affects the acoustic growth rate of the two counter-spinning modes differently. This behavior is expected from the eigenvalue splitting predicted by the theory (Eq. 11). We have shown in §2 that, for a 1D ring with uniform mean flow and constant damping, the co-swirl and counter-swirl components for $M > 0$ should have respectively an acoustic damping rate which is higher and lower than in the zero-Mach number configuration. This is not observed in the experiments, and the normalized growth rate difference is higher than the predicted value, $(\sigma^+ - \sigma^-)/\sigma_{M=0} = 2M$. For example, at $M = 0.025$ the growth rate splitting of the mode 5 is four times greater than the above value. However, for the mode $m = 5$ we indeed observe that the co-swirl component should be more damped than the counter-swirl one, and that the growth rate difference should increase linearly with the Mach number. For $m = 3$ and $m = 4$, at low Mach numbers the co-swirl spinning mode damping rate is enhanced by the azimuthal mean flow to a greater extent than the one of the counter-swirl mode, but increasing the Mach number leads to the opposite behavior for $m = 4$, which makes the acoustic growth rates of the two counter-spinning modes becom-
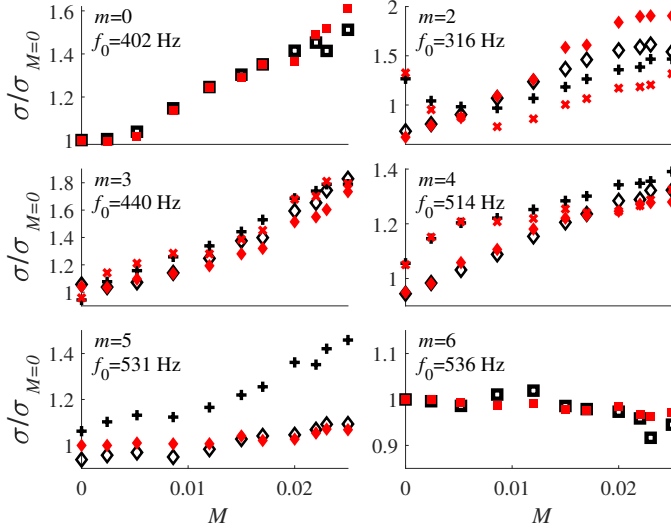
6

FIGURE 3: Ratio of acoustic growth rates as a function of the Mach number. The growth rates are normalized by the mean growth rate at zero Mach number $\sigma_{M=0} = \frac{1}{2}(\sigma_{M=0}^+ + \sigma_{M=0}^-)$. The red and black symbols are obtained with Method 1 and Method 2 (see §1.2), respectively. The crosses and the diamonds represent the co-swirl and the counter-swirl spinning waves, respectively, which do not exist at $m = 0$ and $m = 6$. The frequencies f_0 refer to the $M = 0$ condition.

ing close to each other at high Mach number values. For $m = 3$, at non-small Mach number values, the growth rate difference is almost constant. The growth rate trend of $m = 2$ shows a behavior opposite to the theory, with a counter-swirl mode that is more damped by an increase of M than the co-swirl mode.

Evidently, results based on the one-dimensional Helmholtz equation with uniform mean flow and constant damping do not hold in most of the cases presented. In the case of a straight duct, it is shown in [24] that when the viscous sub-layer thickness becomes comparable to or smaller than the acoustic boundary layer thickness, turbulent damping becomes significant because the turbulence interacts with the acoustic boundary layer. This is observed for high turbulence levels and low frequencies. We estimate, using a result from [24], that for $m = [2, 3, 4, 5, 6]$ the viscous sub-layer thickness becomes smaller than the acoustic boundary layer thickness when the Mach number becomes respectively $M \geq [0.0064, 0.0081, 0.0093, 0.011, 0.012]$, so the turbulent damping should start coming into play from these values of the Mach number. To estimate the wall shear stress, required to estimate the ratio of the acoustic boundary layer and the viscous sub-layer thickness formulated in [24], we used the Blasius formula for the friction factor [25], which uses the assumption of a fully developed turbulent flow in a straight smooth pipe. Notice that this is a very rough estimate and these val-

ues are given only as an order of magnitude estimation, since the geometry is different from that of [24] and the assumption of fully developed flow is questionable, due, for example, to the presence of the fans in the annulus. In addition, in the plane where the annulus/tube connection is, the presence of the tubes prevent the boundary layer to be fully developed. Therefore the use of Blasius formula may lead to overestimate the viscous sub-layer thickness and, consequently, to overestimate the value of Mach number at which turbulent damping becomes significant. However, the conclusion from [24] is qualitatively consistent with the higher sensitivity to an azimuthal flow at low frequencies ($f \leq 440$ Hz) than at higher frequencies ($f \geq 514$ Hz) in the cases presented in Fig. 3, so we suggest that the mismatch can be attributed, at least partially, to turbulent damping.

In [12], for the case of a flame tube, it is demonstrated that the presence of swirl damps the counter-swirl transverse mode stronger than the co-swirl transverse mode. The given explanation is that the wave which travels against the flow encounters more resistance than the wave which travels in the mean flow direction, the interaction between acoustic waves and shear zones being decreased and amplified for the co-swirl and counter-swirl modes, respectively. This intuitive explanation may, in the present study, help understanding the cause for the growth rate splitting of the mode $m = 2$ to be opposite to the splitting behavior predicted by the one-dimensional convective Helmholtz equation. However, the different behavior at various azimuthal mode orders suggest that a single phenomenon is not sufficient to explain all the splitting patterns. This is a combined effect of the mean flow convection that damps the co-swirl mode stronger, the acoustic–shear zone interaction, and the turbulent damping. Also, the presence of the fans at the center of the cavity could create coherent structures that may affect both counter-spinning modes in a different way.

In addition to the combination of the multiple effects described above, the degree of coupling between the chamber mode and tube mode needs to be considered. Since the mean flow is located in the chamber, the Mach number has an effect on the pure chamber modes and not in the pure tube modes. Therefore, a chamber mode weakly coupled with a tube mode will be more sensitive to the azimuthal mean flow than a fully coupled mode of the entire geometry. This would explain why the mode $m = 6$, which has the strongest coupling with the tubes, has an acoustic growth rate that is almost insensitive to the Mach number.

3.2 Damping of self-sustained oscillations due to an azimuthal mean flow

Given the results of §3.1 on the increase of the acoustic damping due to a mean azimuthal flow, one can expect that a mean azimuthal flow is beneficial for the linear stability of annular thermoacoustic systems. Therefore, the effect of a mean azimuthal flow on the self-sustained oscillations is assessed in our

setup with EAF. Experiments are performed at various values of the Mach number by varying the fan input power, for two different initial conditions. The first is an initial state without oscillations: the EAF is initially switched off and then promptly turned on. This is repeated at various values of mean flow velocity. It facilitates studying the effect of the mean flow on linear stability and the resulting impact on the final state. In the second set of experiments, instead, we track the amplitude of the limit cycle oscillations in a quasi-continuous fashion, by slowly increasing the Mach number from 0 to 0.025. The process is then reversed, with the input power decreased towards 0, to study hysteresis effects. The instantaneous value of each complex modal component is obtained by computing the discrete Fourier transform with respect to the azimuthal coordinate at each instant. For each mode, the amplitude curve is then obtained by finding the local maxima of the modal component gain evolution. In this section, no distinction is made between both counter-spinning waves of a given azimuthal order. The linear growth rates are obtained by fitting an exponential envelope proportional to $e^{\sigma t}$ to the modal amplitude curve in the linear regime.

3.2.1 Full suppression of self-sustained oscillations due to an azimuthal mean flow.

In the first case that we present, the flame model parameters are set to $n = 13$ and $\tau = 2.5$ ms. We recall that our definition of n does not correspond directly to a gain from acoustic perturbations to acoustic fluctuations, but it is an amplification factor from voltage (y_j) to voltage (q_j). This value of n should therefore not be thought as high with respect to typical flame gains. The calculation of the overall gain from microphone pressure fluctuations to acoustic fluctuations produced by the loudspeakers would require to multiply n by the conversion factor from pressure fluctuations to microphone voltage signal (5.7×10^{-5} V/Pa) and by the conversion factor from the RTC voltage output to acoustic fluctuations produced by the loudspeaker, which has however not been measured.

The modal amplitude of the periodic oscillations obtained for both types of initial conditions and the experimental linear growth rates as a function of the Mach number are presented in Fig. 4. The only unstable mode is $m = 3$. Its frequency in the absence of azimuthal mean flow is 444 Hz. Figure 4b shows that increasing the Mach number makes the linear growth rate decrease, so that from a Mach number value close to $M = 0.0042$, the system becomes linearly stable. Consequently, no oscillations are observed in Fig. 4a for $M \geq 0.0042$ from a zero-amplitude initial condition. The results obtained with the continuation of limit cycle confirm that an azimuthal mean flow can suppress the oscillations. It is observed that when the Mach number is increased from $M = 0$, a full suppression of the oscillations is obtained at $M = 0.0048$ rather than $M = 0.0042$. This means that between $M = 0.0042$ and $M = 0.0048$ the limit cy-
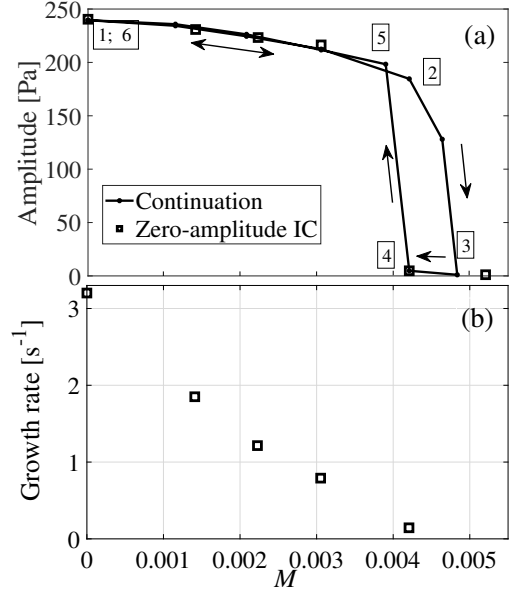

FIGURE 4: Modal pressure amplitude and linear growth rate as a function of the Mach number for $n = 13$ and $\tau = 2.5$ ms. The unstable mode is $m = 3$.

cle corresponding to periodic oscillations of the mode $m = 3$ is still a stable solution, and coexists with the fixed point solution, and that the former becomes unstable or disappears for $M \geq 0.0048$. When the Mach number is slowly decreased, one can observe that until $M = 0.0042$, no oscillations are observed, and that from $M = 0.0039$ to $M = 0$, oscillations are again observed. It is in agreement with the results obtained with the zero-amplitude initial condition. In the lower range of Mach numbers ($M < 0.0039$), the oscillation amplitude follows the same route for the first type of initial condition and for the second type with increasing and with decreasing Mach number.

Consistent with the results of §3.1, this case illustrates the damping effect of an azimuthal mean flow on the self-sustained oscillations. We show that this stabilizing effect can be observed even at low Mach number values.

3.2.2 Mode change due to an azimuthal mean flow.

The flame model parameters are now changed to $n = 3.15$ and $\tau = 2.0$ ms. Contrary to the previous case, two modes are linearly unstable: $m = 4$ and $m = 5$ whose eigenfrequencies are 513 Hz and 529 Hz, respectively. We observe that, when the Mach number is increased, the frequency of each mode decreases only slightly. For both modes, the maximum shift with respect to the $M = 0$ configuration is 0.6 Hz. This behavior is similar to the counter swirl component of the acoustic mode $m = 4$ (fig. 2 in dashed lines). As each frequency does not vary significantly, the frequency gap between the mode $m = 4$ and
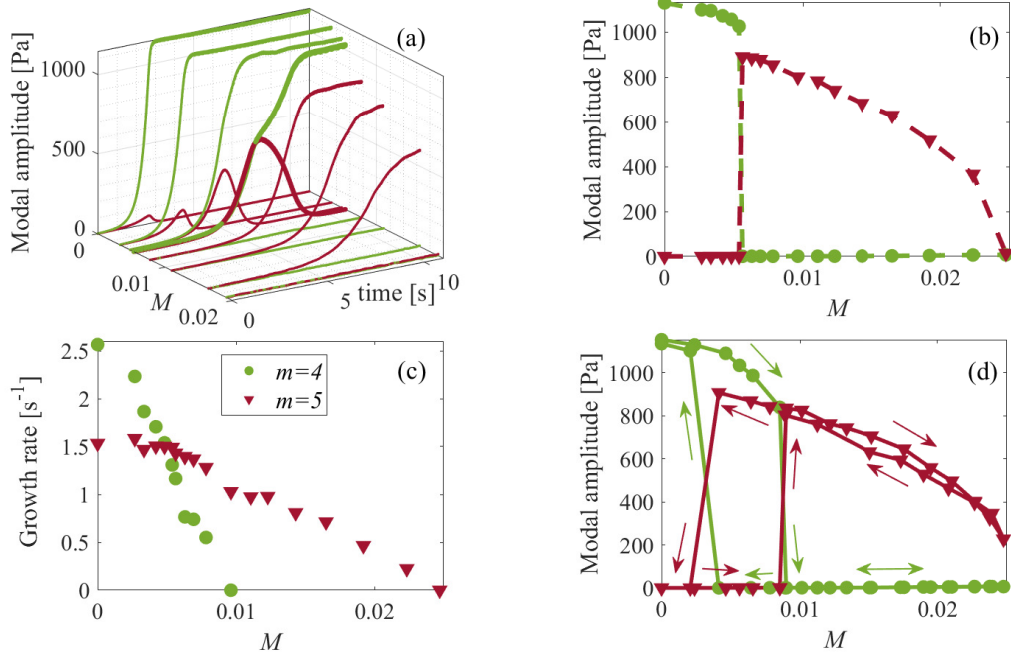
FIGURE 5: Modal pressure amplitude and linear growth rates as a function of the Mach number for $n = 3.15$ and $\tau = 2.0$ ms. The green lines with the circles correspond to $m = 4$, and the red lines with triangles correspond to $m = 5$. (a)–(c) show results obtained with an initial state without oscillations. (d) shows results obtained with a continuation of the limit cycle.

$m = 5$ remains almost constant (~ 16 Hz). The results obtained with the zero-amplitude initial condition and with the continuation of limit cycle are shown in Fig. 5.

The results obtained with the first type of initial condition indicate that, at low Mach number, the linear growth rate of the mode $m = 4$ is significantly higher than that of the mode $m = 5$ (Fig. 5c). Consequently, when nonlinear effects start to affect the oscillations, the amplitude of the mode $m = 4$ is much higher than that of the mode $m = 5$ (Fig. 5a). Finally, we observe periodic oscillations of the 4th-order azimuthal mode (Fig. 5a-b). It is noticed that both the linear growth rates of the mode $m = 4$ and of the mode $m = 5$ decrease when the Mach number increases, and that the former undergoes the sharpest drop. At $M = 0.0054$, the growth rate of the mode $m = 4$ becomes smaller than that of the mode $m = 5$. However, when the nonlinear effects start, the mode $m = 5$ decays while the amplitude of the mode $m = 4$ keeps increasing (Fig. 5a in bold lines). This modal competition scenario leads again to periodic oscillations of the mode $m = 4$. A similar trend, obtained without mean flow, is discussed in [26]. In this case, as well as in other cases where the two growth rates are similar, a transient beating is observed. This is due to the close frequencies of the two mode and the close amplitudes during the exponential growth.

A radical change is observed at higher values of the Mach number. From $M = 0.0056$ on, the mode $m = 5$ is the only one active in the final state, promoted by a favorable growth rate difference that increases with the Mach number. From $M = 0.0096$ on, the mode $m = 4$ becomes linearly stable, while the linear growth rate of the mode $m = 5$ is close to zero at $M = 0.025$. Therefore, for the latter value, no oscillations are observed for a zero-amplitude initial condition.

The effect of initial conditions is assessed in Fig. 5d by performing a continuation of the limit cycle. The experiment starts at zero Mach number. Under this condition, a stable limit cycle oscillation of the mode $m = 4$ is reached. A slow increase of the Mach number until $M = 0.0085$ lowers the oscillation amplitude without changing the mode type. Then, a slight increase of the Mach number ($M = 0.0090$) suppresses the oscillations of the mode 4, giving way to periodic oscillations of the mode $m = 5$. Afterwards, an increase in the Mach number until $M = 0.025$ makes the amplitude of the mode 5 significantly decrease but without suppressing the oscillations. Later, slowly decreasing the Mach number until $M = 0.0041$ leads to an increase of the amplitude without changing the mode number, while a further decrease ($M = 0.0024$) leads to periodic oscillations of the mode 4.

By comparing the final state for various initial conditions, we show that at low Mach number ($M \leq 0.0024$) only one stable solution is found experimentally, while in an intermediate range of Mach numbers ($0.0041 < M < 0.0084$) both periodic oscillations of $m = 4$ and $m = 5$ are stable solutions. The mode that is

actually observed depends on the initial conditions. On the contrary, in the range $0.0090 < M < 0.024$, a limit cycle corresponding to periodic oscillations of the mode $m = 5$ is the only stable solution, due to the fact that the mode $m = 4$ is linearly stable. For $M = 0.025$, the linear growth rate of the mode $m = 5$ being close to zero, no oscillations are observed for a zero-amplitude initial condition, while the oscillations present in the continuation of limit cycles are not suppressed. It is a manifestation of the fact that, in the limit of $\sigma = 0$, the amplitude remains unchanged, by definition.

This case confirms that an azimuthal mean flow has a stabilizing effect on the self-sustained oscillations. In addition, we demonstrate that when multiple modes are linearly unstable, the modal competition scenario can be radically changed by the presence of an azimuthal mean flow with respect to the vanishing Mach number condition. Therefore, for a reliable prediction of the frequency and amplitude of the self-sustained oscillations, one should account for the effects of an azimuthal mean flow.

3.3 Effect of an azimuthal mean flow on the spinning/standing nature of thermoacoustic modes

In §3.2, for each azimuthal mode number, no distinction was made between the two counter-spinning waves. However, it was shown in §3.1 that the mean flow does not have the same effect on both counter-spinning acoustic modes. Therefore, we investigate in this section the effect of an azimuthal mean flow on the spinning/standing nature of thermoacoustic modes. Three cases obtained with different flame model parameters are presented. Both types of initial conditions presented earlier are used. The amplitudes of both counter-spinning components of the dominant azimuthal mode are extracted by projecting the complex pressure profile, obtained from the Hilbert transform of the pressure signal from each microphone, on the spinning wave basis [16]. Their values in the final state are compared in Fig. 6. In what follows, for each case (a, b and c), we refer to the numbers labeled in Fig. 6 to describe the main steps of the continuation of limit cycles. The linear growth rates are not shown but, in these cases, for the zero-amplitude initial condition, the mode with the highest linear growth rate is dominant in the final state.

In case (a) the flame model parameters are set to $n = 13$ and $\tau = 2.3$ ms. The dominant mode is $m = 3$. For the first type of initial condition (no oscillation in the initial state), it can be seen that at low Mach number, the counter-swirl mode dominates in the final state while for $M \geq 0.0041$ the co-swirl spinning mode becomes dominant. When performing a continuation of limit cycles, these observations still stand at low Mach number values ($M < 0.002$) and in a higher range of Mach numbers ($M > 0.011$), but the modal amplitude behavior is more complex in an intermediate range of mean flow velocities due to the presence of hysteresis. Given the counter-swirl spinning nature of the mode at low Mach number (point (1) in Fig. 6 case (a)),

increasing the Mach number up to 0.01 (2) is not sufficient to change the spinning direction. Then, a further increase in Mach number leads to a co-swirl spinning mode (3), and this mode nature is conserved at higher Mach number values (4). Afterwards, when decreasing the Mach number from (4), the dominant mode remains co-swirl spinning until $M = 0.0027$ (6) while a further decrease leads again to a counter-swirl spinning mode (7). The fact that the mean flow promotes the co-swirl spinning mode is not expected from acoustic growth rate results shown in Fig. 3. However, knowing that the mean flow splits the acoustic eigenfrequencies, one can expect that, for a given acoustic growth rate, when the thermoacoustic feedback of a flame (EAF in our case) is introduced, the two acoustic poles will not be moved the same way by the flame transfer function. In other words, the mode that has the highest thermoacoustic growth rate is not necessarily found to be the one that has the largest acoustic growth rate.

In case (b) the flame model parameters are changed to $n = 13$ and $\tau = 0.3$ ms. The unstable mode is $m = 4$. Both types of initial conditions lead to the same results, without hysteresis phenomenon. At very low Mach number ($M \leq 0.0024$) the modes are dominantly standing. Two nodal lines are aligned with the tubes. Increasing the Mach number leads to a dominant counter-swirl mode. This is consistent with the acoustic growth rate behavior shown in Fig. 3. However, from Fig. 3, one could have expected to observe also a dominantly "counter-swirl" mode at $M = 0$. Here we do not observe the presence of a stable co-swirl spinning solution at any value of M, but its absence is not proved.

In case (c), $n = 3.15$ and $\tau = 1.9$ ms, the unstable mode is $m = 5$. The results obtained with the zero-amplitude initial condition indicate that at low Mach number, the dominant mode is co-swirl spinning. At intermediate Mach number values we observe cases for which the co-swirl and counter-swirl component have similar amplitudes. At $M = 0.0061$, the oscillations result from the superposition of various modes of different but very close frequencies. Since the two main components have a frequency spacing of 0.3 Hz, beating oscillations with an amplitude modulation is observed. At $M = 0.0076$ we observe only one frequency of oscillations; it corresponds to a dominantly standing mode. One nodal line passes at the middle between tubes. For higher Mach number values, the spinning mode propagating against the mean flow dominates. The preference for the counter-swirl mode is consistent with the Mach number dependence of the acoustic growth rates shown in Fig. 3. However, performing the continuation of limit cycles starting with a dominant co-swirl spinning mode at $M = 0$ (1), when the Mach number is slowly increased until $M = 0.025$ (2), the mode nature is not affected. Then, the operation is reversed, by starting the EAF at $M = 0.025$, leading to a dominant counter-swirl mode (3). Decreasing the Mach number until $M = 0.0078$ does not change the spinning direction, while at $M = 0.0067$ a standing mode with a nodal line passing at the middle between tubes is observed; a further decrease leads to a dominant co-swirl spinning mode.
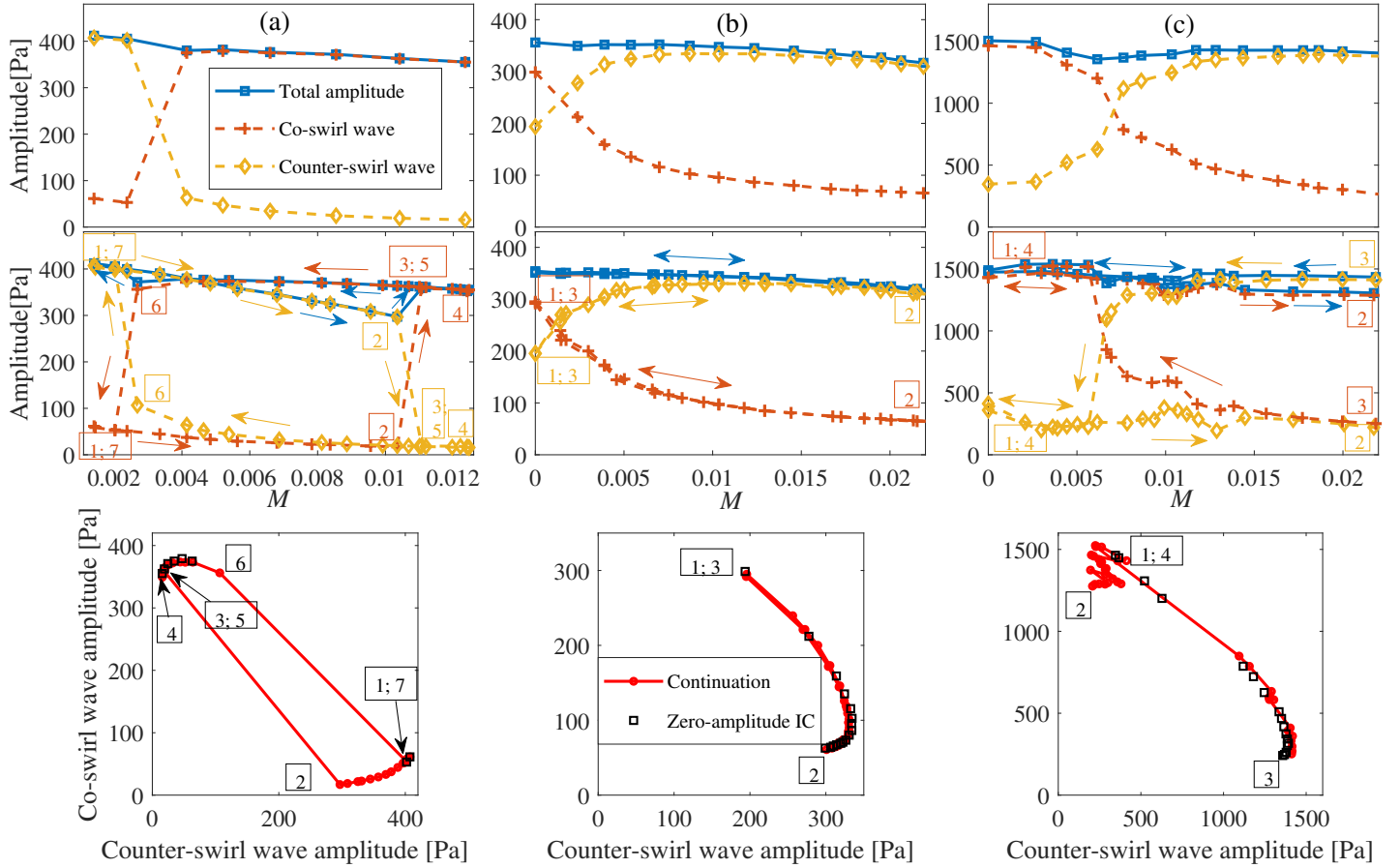
FIGURE 6: Influence of the Mach number on the mode nature in the final state. The first two rows show the co-swirl and counter-swirl spinning components and the total amplitude as a function of M, for the zero-amplitude initial condition (top) and for the continuation of the limit cycle (middle). Bottom row: Final state for both types of initial conditions. Left (a): $n = 13$, $\tau = 2.3$ ms (mode $m = 3$), middle (b): $n = 13$, $\tau = 0.3$ ms (mode $m = 4$), right (c): $n = 3.15$, $\tau = 1.9$ ms (mode $m = 5$).

This behavior illustrates the presence of hysteresis, as in case (a) but on a wider range of Mach numbers, in which both counter-spinning modes are stable solutions. The Mach number that defines the upper limit of the hysteresis is larger than $M = 0.025$. Therefore it cannot be determined experimentally with the fans used in this study.

We discuss these results in view of the theoretical model of [10] based on a low-order wave-based representation of the thermoacoustic interaction in a perfectly axisymmetric 1D annulus with a continuous distribution of flames, with a uniform azimuthal mean flow, and with a cubic saturation term. In [10], at low Mach number and with an axisymmetric distribution of flames, the only stable solutions predicted by the model are the two counter-spinning modes. On the contrary, at higher Mach number values only the counter-spinning mode is predicted to be stable, favored by a larger linear growth rate due to convective effects. However, in the vanishing Mach number limit our results

do not all confirm this prediction: we find spinning, standing and mixed modes. This difference may be attributed to an imperfect symmetry and/or to different nonlinear saturation mechanisms. Moreover, we found cases at non-zero Mach numbers for which the two counter-spinning modes have similar amplitudes: it can be a dominantly standing mode (b and c) or a combination of modes of distinct but close frequencies (c). In an intermediate range of Mach numbers in case (a) and (c) we indeed find two stable solutions, close to spinning, whereas for case (b) only one solution is observed (counter-swirl spinning mode), but this does not necessarily imply that the co-swirl spinning mode is not a stable solution. The fact that in a higher range of Mach numbers only one spinning solution is predicted to be stable is consistent with cases (a) and (b). For case (c), we cannot reach a conclusion on the uniqueness of a stable solution because, at full fan power, two stable solutions still exist, but considering the results obtained with the continuation of limit cycles, one can imagine

that only the counter-swirl mode remains stable from a critical Mach number that would determine the upper end of the hysteresis region. Nevertheless, in contrast to [10], we found that the spinning direction promoted by the azimuthal mean flow is not necessarily counter-swirl spinning. As previously discussed this may be due to the effects of turbulent damping and acoustic–shear zone interaction, not taken into account in the model, and to the fact that it is not necessarily the mode with the largest acoustic growth rate that has the highest thermoacoustic growth rate, as the frequency splitting may have a significant effect on stability of each mode independently. We conclude noting that also the difference in the geometry (so in the complexity of the modes) and in the nonlinear model (saturation limit in this study and cubic saturation in [10]) may explain some discrepancies.

CONCLUSION

This article addresses the effects of an azimuthal mean flow on the acoustic modes and on the self-sustained oscillations in an annular setup with electroacoustic feedback. The flexibility of the electroacoustic feedback allows to choose flame model parameters that lead to characteristics of interest while the electrically powered fans allow to continuously vary the mean azimuthal flow in a wide and realistic range of Mach numbers.

We confirmed experimentally that an azimuthal mean flow splits the acoustic – and consequently thermoacoustic – eigenvalues, and demonstrated that it increases the acoustic damping. The azimuthal flow effects on acoustic and thermoacoustic modes include convective effects due to the bulk flow, turbulence effects and acoustic–shear zone interaction. Their effects depend on the mode frequency and on the propagation direction. Convective effects damp more the co-swirl spinning wave while acoustic–shear zone interactions presumably damp more the counter-swirl component. Turbulent damping has a greater effect at low frequencies [24]. Moreover, these effects, located in the chamber, affect the fully coupled modes of the entire geometry to a lower extent than the chamber modes weakly coupled with the tube modes. The diversity of the observed splitting patterns may be attributed to the combination of these various damping effects and to the degree of coupling between the chamber and tube modes.

We demonstrated that a mean azimuthal flow has a stabilizing effect on the self-sustained oscillations, even at low Mach numbers. We envisage that this may lead to new ideas in the design of thermoacoustically stable industrial annular combustors. We point out that, when multiple modes are linearly unstable, an azimuthal mean flow plays a major role in the modal competition. Therefore, a reliable prediction of the frequency and amplitude of the self-sustained oscillations requires to take the azimuthal mean flow into account.

It was demonstrated that an azimuthal mean flow promotes spinning modes, or mixed-modes close to spinning at sufficiently high Mach number values, while in a narrow range of Mach numbers standing modes may also be encountered. Moreover, due to the frequency splitting caused by the mean flow, a beating behavior has been observed. No general conclusion about the preferred spinning direction could be drawn, first of all because not all the acoustic modes are affected by the mean flow in the same manner. We also suggest that the acoustic growth rate gap between both counter-spinning modes is not necessarily the only responsible for the difference of thermoacoustic growth rates. We conjecture that the frequency splitting may also have a significant effect on the thermoacoustic growth rate.

REFERENCES

[1] Lieuwen, T. C., 2012. *Unsteady Combustor Physics*. Cambridge University Press.

[2] Candel, S., 2002. "Combustion dynamics and control: Progress and challenges". *P Combust Inst, 29*(1), pp. 1–28.

[3] Staffelbach, G., Gicquel, L. Y., Boudier, G., and Poinsot, T., 2009. "Large eddy simulation of self-excited azimuthal modes in annular combustors". *P Combust Inst, 32*(2), pp. 2909–2916.

[4] Wolf, P., Staffelbach, G., Gicquel, L. Y., Müller, J.-D., and Poinsot, T., 2012. "Acoustic and large eddy simulation studies of azimuthal modes in annular combustion chambers". *Combust Flame, 159*(11), pp. 3398–3413.

[5] Bourgoin, J.-F., Durox, D., Schuller, T., Beaunier, J., and Candel, S., 2013. "Ignition dynamics of an annular combustor equipped with multiple swirling injectors". *Combust Flame, 160*(8), pp. 1398–1413.

[6] Worth, N. A., and Dawson, J. R., 2013. "Modal dynamics of self-excited azimuthal instabilities in an annular combustion chamber". *Combust Flame, 160*(11), pp. 2476–2489.

[7] Nygard, H. T., Mazur, M., Dawson, J. R., and Worth, N. A., 2019. "Flame dynamics of azimuthal forced spinning and standing modes in an annular combustor". *P Combust Inst, 37*(4), pp. 5113–5120.

[8] Bauerheim, M., Cazalens, M., and Poinsot, T., 2015. "A theoretical study of mean azimuthal flow and asymmetry effects on thermo-acoustic modes in annular combustors". *P Combust Inst, 35*(3), pp. 3219–3227.

[9] Rouwenhorst, D., Hermann, J., and Polifke, W., 2017. "Bifurcation study of azimuthal bulk flow in annular combustion systems with cylindrical symmetry breaking". *Int J Spray Combust, 9*(4), pp. 438–451.

[10] Faure-Beaulieu, A., and Noiray, N., 2020. "Symmetry breaking of azimuthal waves: Slow-flow dynamics on the Bloch sphere". *Phys Rev Fluids, 5*(2), p. 023201.

[11] Fleury, R., Sounas, D. L., Sieck, C. F., Haberman, M. R., and Alù, A., 2014. "Sound isolation and giant linear non-reciprocity in a compact acoustic circulator". *Science, 343*(6170), pp. 516–519.

[12] Hummel, T., Berger, F., Schuermans, B., and Sattelmayer, T., 2016. "Theory and modeling of non-degenerate transversal thermoacoustic limit cycle oscillations". *Thermoacoustic Instabilities in Gas Turbines and Rocket Engines: Industry meets Academia*, pp. 271–290.

[13] Humbert, S. C., Gensini, F., Andreini, A., Paschereit, C. O., and Orchini, A., 2020. Nonlinear analysis of self-sustained oscillations in an annular combustor model with electroacoustic feedback. Accepted to the 38th International Symposium on Combustion.

[14] Noiray, N., and Schuermans, B., 2012. "Theoretical and experimental investigations on damper performance for suppression of thermoacoustic oscillations". *J Sound Vib, 331*(12), pp. 2753–2763.

[15] Noiray, N., and Schuermans, B., 2013. "Deterministic quantities characterizing noise driven Hopf bifurcations in gas turbine combustors". *J Nonlin Mech, 50*, pp. 152–163.

[16] Moeck, J., 2010. "Analysis, modeling, and control of thermoacoustic instabilities". PhD Thesis, Technische Universität Berlin.

[17] Moeck, J. P., Paul, M., and Paschereit, C. O., 2010. "Thermoacoustic instabilities in an annular Rijke tube". *ASME Turbo Expo, GT2010-23577*, pp. 1219–1232.

[18] Gelbert, G., Moeck, J. P., Paschereit, C. O., and King, R., 2012. "Feedback control of thermoacoustic modes in an annular Rijke tube". *Control Eng Pract, 20*(8), pp. 770–782.

[19] Munson, B. R., Young, D. F., Okiishi, T. H., and Huebsch, W. W., 2009. *Fundamentals of Fluid Mechanics, 6th Edition*. John Wiley & Sons, Inc.

[20] Palies, P., Durox, D., Schuller, T., and Candel, S., 2011. "Nonlinear combustion instability analysis based on the flame describing function applied to turbulent premixed swirling flames". *Combust Flame, 158*(10), pp. 1980–1991.

[21] Gustavsen, B., and Semlyen, A., 1999. "Rational approximation of frequency domain responses by vector fitting". *IEEE Trans. Power Delivery, 14*(3), pp. 1052–1061.

[22] Crocco, L., and Cheng, S., 1956. "Theory of combustion instability in liquid propellant rocket motors". *AGARDograph, 8*.

[23] Dowling, A., 1997. "Nonlinear self-excited oscillations of a ducted flame". *J Fluid Mech, 346*, pp. 271–290.

[24] Weng, C., Boij, S., and Hanifi, A., 2013. "Sound-turbulence interaction in low Mach number duct flow". *19th AIAA/CEAS Aeroacoustics Conference*.

[25] Blasius, P. R. H., 1913. "Das Aehnlichkeitsgesetz bei Reibungsvorgängen in Flüssigkeiten". *Verein deutscher Ingenieure (eds) Mitteilungen über Forschungsarbeiten auf dem Gebiete des Ingenieurwesens, 131*, pp. 1–41.

[26] Moeck, J. P., and Paschereit, C. O., 2012. "Nonlinear interactions of multiple linearly unstable thermoacoustic modes". *Int J Spray Combust, 4*(1), pp. 1–28.